International Journal of Control and Automation
Vol.10, No.7 (2017), pp.217-228
http://dx.doi.org/10.14257/ijca.2017.10.7.18

Modified Unscented Kalman Filter for XNAV with Dynamic Model Uncertainties in Earth-Mars Transfer Orbit

Xiaoyu Li, Jin Jing, Xiao Chen and Yi Shen

Department of Control Science and Engineering,
Harbin Institute of Technology, Harbin
jinjinghit@hit.edu.cn

Abstract

This paper presents a modified strong tracking unscented Kalman filter (MSTUKF) to deal with the dynamical model uncertainties including the model mismatch and abnormal unknown disturbance in the X-ray pulsar based navigation system. The MSTUKF adopts the statistical information to establish system state detection function and further introduce the fading factor in the prediction covariance so that the filter gain of MSTUKF can be revised. Then, the performance of MSTUKF filtering algorithm is tested and compared with the other three filtering methods. Simulation results show he proposed method can achieve better performance and effectively decrease the impact of the model uncertainties to navigation system.

Keywords: *XNAV, model uncertainties, UKF, MSTUKF*

1. Introduction

X-ray pulsar-based navigation (XNAV) is a new autonomous celestial navigation technology [1]. Compared with the other navigation methods, XNAV has the advantage of high reliability, high precision and strong autonomy [2]. Thus, the XNAV method has become a hot subject in the spacecraft autonomous navigation field [3].

The XNAV relies on X-ray sensors which fixed in the spacecraft, the pulsed signal's time of arrival (TOA) can be detected by the sensors after a period of observation (usually 5-10 min) [4]. Meanwhile, the pulsar's TOA at the solar system barycenter (SSB) can be accurately obtained based on the pulsar timing model. Thus, the offset of the TOA at the spacecraft compared to its corresponding time at the SSB can be regarded as the measurement of the XNAV. Combined with the dynamical model, the navigation information of the spacecraft can be obtained by the filtering algorithm.

EKF [5-6] is a commonly used filtering algorithm for nonlinear estimation. The dynamical model is obtained by the Taylor expansion. However, truncation error exists due to the omission of the high order term. The UKF [7-9] based method reduces the nonlinear error by approximating the probability density of state distribution via the unscented transform (UT) which is suitable for nonlinear estimation. Compared with the EKF, UKF avoids the truncation error and the calculation of Jacobian matrix.

However, in the cruise phase of earth-mars transfer orbit, the spacecraft orbit can change greatly in short time due to the uncertainties of orbit dynamical model and the abnormal disturbance of unknown planetary, such as comets, asteroids or the satellites of planetary. As the pulsar signal usually takes a long time to accumulate the pulse profile to obtain a higher accuracy of the measurement value. Thus, the XNAV usually spends several minutes on the whole filtering procedure. When the orbit changes greatly in short time, large estimation errors will occur in the XNAV. In addition, the accumulation of estimation errors will lead to the divergence of filtering algorithm.

In order to save the problem, adaptive unscented Kalman filter [10] (AUKF) and strong tracking unscented Kalman filter [11] are developed. The performances of the two filters

ISSN: 2005-4297 IJCA

are improved by the adaptive factor and suboptimal factor respectively. However, the adaptive factor is calculated in the whole filter procedure, decreasing the precision in case of the dynamical model without uncertainty.

In this paper, a modified strong tracking unscented Kalman filter (MSTUKF) algorithm is developed for XNAV in presents of dynamical model uncertainty. The dynamical model uncertainty is identified via the statistical information. In addition, the idea of strong tracking method is introduced to deal with the abnormal dynamical model uncertainty based on the calculated fading factor in prediction covariance so that the Kalman gain matrix can be revised.

This paper is organized as follows. In Section 2, the navigation system model of XNAV is given and the system bias caused by the dynamical model uncertainties is analyzed. In Section 3, the proposed navigation method based on MSTUKF is designed. The effectiveness of the proposed method is demonstrated through simulations in Section 4. Finally, the conclusions are drawn in Section 5.

2. Navigation System Model and Filtering Error Analysis

2.1. Measurement Model

The principle of XNAV is described in Figure 1. The transfer orbit phase of XNAV is from point A to point B. The XNAV's observation is obtained by processing the offset of TOA between the SSB and spacecraft. $\boldsymbol{R}_{SC}$ is the position vector of spacecraft with respect to SSB. The offset of Δt is described as:

$$z_i = c\Delta t^i = c(t_{SSB}^i - t_{SC}^i) = \boldsymbol{n}_i \boldsymbol{R}_{SC} \tag{1}$$

where c is the speed of light, $\boldsymbol{n}_i$ is the pulsar direction of the i th pulsar. $\boldsymbol{n}_i = [\cos\delta^i \sin\alpha^i \quad \cos\delta^i \cos\alpha^i \quad \sin\delta^i]$, α^i and δ^i are the right ascension and declination of the i th pulsar, respectively. Thus, the measurement model is defined as:

$$\boldsymbol{z}_k = \boldsymbol{H}_k \boldsymbol{x}_k + \boldsymbol{V}_k \tag{2}$$

where $\boldsymbol{H}_k$ is the measurement matrix, according to (1), $\boldsymbol{H}_k = [\boldsymbol{n}_{i\times 3} \quad \boldsymbol{0}_{i\times 3}]$. i is the number of adopted pulsars, in this paper, $i = 3$. $\boldsymbol{V}_k$ is the measurement noise.

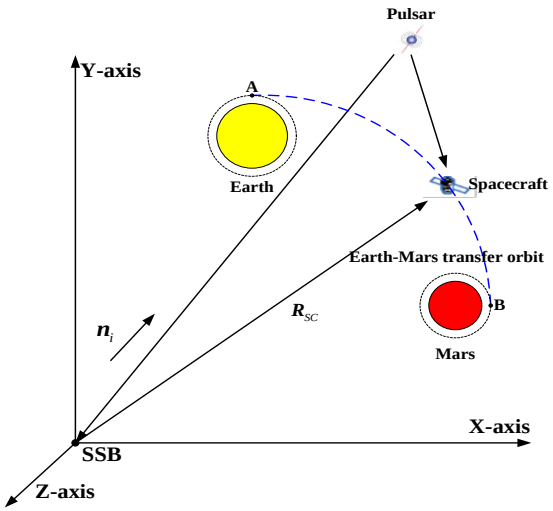

Figure 1. The Principle of X-ray Pulsar Measurement

2.2. Dynamical Model

For the Earth-Mars transfer orbit, the gravity of Sun, Earth and Mars are considered. Thus, the The dynamical model is established based on the three-body equation of motion which is is described as:

$$\begin{cases} \dot{\boldsymbol{r}} = \boldsymbol{v} + \boldsymbol{w}_r \\ \dot{\boldsymbol{v}} = -\mu_s \dfrac{\boldsymbol{r}_{ps}}{r_{ps}^3} - \mu_m \left(\dfrac{\boldsymbol{r}_{pm}}{r_{pm}^3} - \dfrac{\boldsymbol{r}_{sm}}{r_{sm}^3} \right) - \mu_e \left(\dfrac{\boldsymbol{r}_{pe}}{r_{pe}^3} - \dfrac{\boldsymbol{r}_{se}}{r_{se}^3} \right) + \boldsymbol{w}_v \end{cases} \tag{3}$$

where $\boldsymbol{r} = [x \quad y \quad z]^T$ and $\boldsymbol{v} = [v_x \quad v_y \quad v_z]^T$ are the position vector and velocity vector. μ_s, μ_m, μ_e are the gravitational constant of Sun, Mars and Earth, respectively. The corresponding values are $1.32 \times 10^{11} \mathrm{km}^3/\mathrm{s}^2$, $3.98 \times 10^5 \mathrm{km}^3/\mathrm{s}^2$, $4.28 \times 10^4 \mathrm{km}^3/\mathrm{s}^2$. $\boldsymbol{r}_{ps}$, $\boldsymbol{r}_{pm}$, $\boldsymbol{r}_{pe}$ are the position vector with respect to SSB, Mars and Earth. $\boldsymbol{r}_{sm}$ and $\boldsymbol{r}_{se}$ are the position vector from SSB to Mars and Earth which is predicted by the emphasis which can be obtained by JPL's DE405. $\boldsymbol{w} = [\boldsymbol{w}_r \quad \boldsymbol{w}_v]^T$ is the process noise which obeys the Gaussian distribution with zeros mean.

2.3. Observability Analysis

According to 2.1 and 2.2, the XNAV is composed by (2) and (3) and written in general as:

$$\begin{cases} \boldsymbol{x}_k = f(\boldsymbol{x}_{k-1}) + \boldsymbol{w}_k \\ \boldsymbol{y}_k = \boldsymbol{H}_k \boldsymbol{x}_k + \boldsymbol{V}_k \end{cases} \tag{4}$$

where $\boldsymbol{x}_k \in \mathbf{R}^n$ and $\boldsymbol{z}_k \in \mathbf{R}^n$ are the system state and the measurement vectors. $f(\square)$ is the nonlinear function in the dynamical model. $\boldsymbol{w}_k$ and $\boldsymbol{V}_k$ are the process and measurement noise with the covariance $\boldsymbol{Q}_k$ and $\boldsymbol{R}_k$ respectively. Thus, the observability is defined as:

$$\boldsymbol{O}_k = [\boldsymbol{H}_k \quad \boldsymbol{H}_k \boldsymbol{F}_k] \tag{5}$$

where $\boldsymbol{F}_k$ is the state transition matrix which is defined as:

$$\boldsymbol{F}_k = \left. \frac{\partial f(x(t))}{\partial x(t)} \right|_{x(t)=x_k} = \begin{bmatrix} \boldsymbol{0}_{3\times3} & \boldsymbol{I}_{3\times3} \\ \boldsymbol{S}_k & \boldsymbol{0}_{3\times3} \end{bmatrix} \tag{6}$$

and $\boldsymbol{S}_k$ can be approximately described as:

$$\begin{cases} S_k(1,1) = \mu_s(1/r^3 - 3x^2/r^5) - \mu_m(1/r_{pm}^3 - 3(r_{pm,x})^3/r_{pm}^5) - \mu_e[1/r_{pe}^3 - 3(r_{pe,x})^3/r_{pe}^3] \\ S_k(1,2) = 3\mu_s(xy/r^5) + 3\mu_m(r_{pm,x}r_{pm,y}/r_{pm}^5) + 3\mu_e(r_{pe,x}r_{pe,y}/r_{pe}^5) \\ S_k(1,3) = 3\mu_s(xz/r^5) + 3\mu_m(r_{pm,x}r_{pm,z}/r_{pm}^5) + 3\mu_e(r_{pe,x}r_{pe,z}/r_{pe}^5) \\ S_k(2,1) = 3\mu_s(xy/r^5) + 3\mu_m(r_{pm,x}r_{pm,y}/r_{pm}^5) + 3\mu_e(r_{pe,x}r_{pe,y}/r_{pe}^5) \\ S_k(2,2) = \mu_s(1/r^3 - 3x^2/r^5) - \mu_m(1/r_{pm}^3 - 3(r_{pm,y})^3/r_{pm}^5) - \mu_e[1/r_{pe}^3 - 3(r_{pe,y})^3/r_{pe}^3] \\ S_k(2,3) = 3\mu_s(yz/r^5) + 3\mu_m(r_{pm,y}r_{pm,z}/r_{pm}^5) + 3\mu_e(r_{pe,y}r_{pe,z}/r_{pe}^5) \\ S_k(3,1) = 3\mu_s(xz/r^5) + 3\mu_m(r_{pm,x}r_{pm,z}/r_{pm}^5) + 3\mu_e(r_{pe,x}r_{pe,z}/r_{pe}^5) \\ S_k(3,2) = 3\mu_s(yz/r^5) + 3\mu_m(r_{pm,y}r_{pm,z}/r_{pm}^5) + 3\mu_e(r_{pe,y}r_{pe,z}/r_{pe}^5) \\ S_k(3,3) = \mu_s(1/r^3 - 3x^2/r^5) - \mu_m(1/r_{pm}^3 - 3(r_{pm,z})^3/r_{pm}^5) - \mu_e[1/r_{pe}^3 - 3(r_{pe,z})^3/r_{pe}^3] \end{cases} \tag{6}$$

Obviously, $rank(\boldsymbol{O}_k) = 6$. The navigation system is completely observable.

2.4. UKF and its Error Analysis

The procedure of UKF based method is described as follows:

Step 1: Initialization

In UKF, the state vector $\boldsymbol{x}_{k-1}$ of XNAV with the mean $\hat{\boldsymbol{x}}_{k-1}$ and covariance $\hat{\boldsymbol{P}}_{k-1}$, the sigma point in UT transform is processed as follows:

$$\begin{cases} \boldsymbol{\chi}_{i,k-1} = \hat{\boldsymbol{x}}_{k-1} & i = 0 \\ \boldsymbol{\chi}_{i,k-1} = \hat{\boldsymbol{x}}_{k-1} + (a\sqrt{n\hat{\boldsymbol{P}}_{k-1}})_i & i = 1,...,n \\ \boldsymbol{\chi}_{i,k-1} = \hat{\boldsymbol{x}}_{k-1} - (a\sqrt{n\hat{\boldsymbol{P}}_{k-1}})_{i-n} & i = n+1,...,2n \end{cases} \tag{5}$$

where $(a\sqrt{n\hat{\boldsymbol{P}}_{k-1}})_i$ is the i th column of the matrix $\sqrt{n\hat{\boldsymbol{P}}_{k-1}}$, a is the parameter, in this paper, a is set to 0.1.

Step 2: Prediction

Each sigma point is processed with the dynamical model in (4).

$$\boldsymbol{\chi}_{i,k/k-1} = f(\boldsymbol{\chi}_{i,k-1}) \tag{6}$$

The predicted mean and covariance is written as:

$$\hat{\boldsymbol{x}}_{k/k-1} = \sum_{i=0}^{2n} \omega_i \boldsymbol{\chi}_{i,k/k-1} \tag{7}$$

$$\hat{\boldsymbol{P}}_{k/k-1} = \sum_{i=0}^{2n} \omega_i (\boldsymbol{\chi}_{i,k/k-1} - \hat{\boldsymbol{x}}_{k/k-1})(\boldsymbol{\chi}_{i,k/k-1} - \hat{\boldsymbol{x}}_{k/k-1})^T + \boldsymbol{Q}_k \tag{8}$$

where $\begin{cases} \omega_i = 1-(1/a^2) & i = 0 \\ \omega_i = 1/2na^2 & i = 1,...,2n \end{cases}$.

Step 3: Measurement update

As the measurement model of XNAV is linear, the step 3 is summarized as follows:

$$\hat{\boldsymbol{z}}_{k/k-1} = \boldsymbol{H}_k \hat{\boldsymbol{x}}_{k/k-1} \tag{9}$$

$$\hat{\boldsymbol{P}}_{zz} = \boldsymbol{H}_k \hat{\boldsymbol{P}}_{k/k-1} \boldsymbol{H}_k^T + \boldsymbol{R}_k \tag{10}$$

$$\hat{\boldsymbol{P}}_{xz} = \hat{\boldsymbol{P}}_{k/k-1} \boldsymbol{H}_k^T \tag{11}$$

$$\boldsymbol{K}_k = \hat{\boldsymbol{P}}_{xz} \hat{\boldsymbol{P}}_{zz}^{-1} \tag{12}$$

$$\hat{\boldsymbol{x}}_k = \hat{\boldsymbol{x}}_{k/k-1} + \boldsymbol{K}_k (\boldsymbol{z}_k - \hat{\boldsymbol{z}}_{k/k-1}) \tag{13}$$

$$\hat{\boldsymbol{P}}_k = \hat{\boldsymbol{P}}_{k/k-1} - \boldsymbol{K}_k \hat{\boldsymbol{P}}_{zz} \boldsymbol{K}_k^T \tag{14}$$

However, in real earth-mars transfer orbit, the spacecraft is far from the Jupiter in the initial phase. The gravity of other celestial body must be taken into consideration in case that the spacecraft encounters with Jupiter and other celestial bodies. If the mismatched dynamical model is utilized in (4), the performance of UKF algorithm will decrease, which is shown in Figure 2. If the mismatched dynamical model is adopted, the position estimation error is slowly increased to 4×10^3 m, the velocity estimation error is increased to 0.5 m/s. the accumulation of estimation error leads to the decrease of UKF's performance.

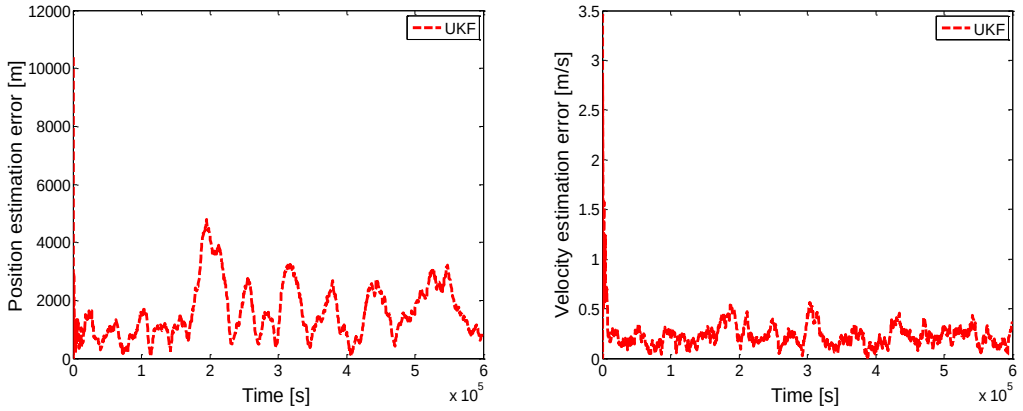

Figure 2. System Bias in Dynamical Model

Besides the dynamical model mismatch, abnormal disturbance is another dynamical model uncertainty factor. In the cruise phase of earth-mars transfer orbit, the spacecraft may encounter with the asteroid, satellites of the Mars or comets, making the abnormal disturbance exist in short time. Suppose the earth-mars transfer orbit started from 1997.07.01.12:00:00.0000, the abnormal disturbance occurs in the 2×10^5 seconds. The performance of UKF is shown in Figure 3. When the spacecraft encounter with the Jupiter, the position estimation error increases to 4000 m and the velocity estimation error increases to 0.5 m/s, respectively. The performance of UKF is obviously decreased in presents of the abnormal disturbance.

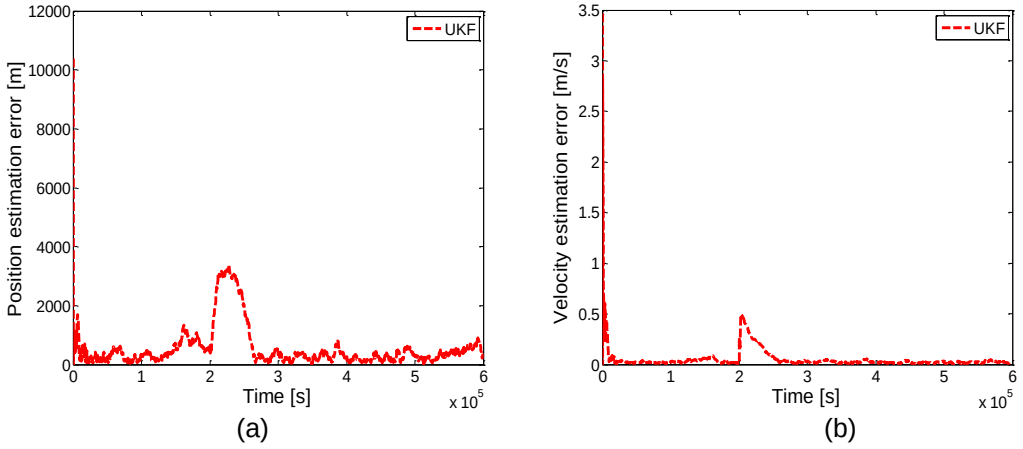

Figure 3. System Bias in Dynamical Model

As can be seen from the above analysis, the model mismatch and abnormal disturbance will severely decrease the performance of UKF. The reason is that the measurement residual $\boldsymbol{e}_k = \boldsymbol{z}_k - \hat{\boldsymbol{z}}_{k/k-1}$ will increase in case that the model mismatch or abnormal disturbance occurs. The filter gain $\boldsymbol{K}_k$ of UKF cannot revise the change of $\boldsymbol{e}_k$. Thus, the conventional UKF filtering algorithm must be modified so that the abnormal disturbance can be detected and the change of measurement residual $\boldsymbol{e}_k$ can be revised.

3. Proposed Navigation Filtering Algorithm

Based on the error analysis of UKF, the dynamical model uncertainties must be detected and the corresponding filtering algorithm must be designed to cope with the problem which affects the accuracy of navigation system. In this paper, the ideal with strong tracking filtering and system state detection function is proposed. The system state detection function can identify the influence to XNAV. The strong tracking filtering can deal with the dynamical uncertainties.

3.1. System State Detection Function

In order to detect the model uncertainty, the theory of hypothesis testing is adopted and the following two hypotheses are defined:

$\boldsymbol{H}_0$: The system is normally operating.

$\boldsymbol{H}_1$: Abnormal exists in the system.

As illustrated in 2.3, the measurement residual can effectively reflect the sensitively change in case of dynamical uncertainties. Thus, the detection function is based on the measurement residual and the corresponding covariance. Define the detection function as:

$$\boldsymbol{F}_k = \boldsymbol{e}_k^T (\boldsymbol{H}_k \hat{\boldsymbol{P}}_{k/k-1} \boldsymbol{H}_k^T + \boldsymbol{R}_k)^{-1} \boldsymbol{e}_k \tag{15}$$

where the statistical function of $\boldsymbol{F}_k$ obeys the $\boldsymbol{\chi}^2$ distribution with m degrees of freedom. The threshold $\chi^2_{a,m}$ can be determined based on the given significance $f(0 < p \le 1)$ and the following relationship:

$$P(\chi^2 > \chi^2_{a,m}) = p \tag{16}$$

If the statistical function $\boldsymbol{F}_k$ is larger than the threshold $\chi^2_{a,m}$, the hypothesis $\boldsymbol{H}_1$ is correct which means the abnormal exists in the system.

$\boldsymbol{H}_0$: $\boldsymbol{F}_k \le \chi^2_{a,m} \quad \forall k$.

$\boldsymbol{H}_1$: $\boldsymbol{F}_k > \chi^2_{a,m} \quad \exists k$.

In this paper, the degree of freedom m is 3, the significance p is 0.01, in the chi-distribution table, the threshold $\chi^2_{a,m}$ is 11.345.

3.2. Modified Strong Tracking Unscented Kalman Filter Algorithm

The main ideal of strong tracking filter is to introduce the suboptimal into the prediction covariance so that the filter gain can be revised in real-time and further improve the ability to cope with the dynamical model uncertainty. Thus, the modified prediction covariance in MSTUKF is defined as:

$$\hat{\boldsymbol{P}}^*_{k/k-1} = \boldsymbol{\lambda}_k \sum_{i=0}^{2n} \omega_i (\boldsymbol{\chi}_{i,k/k-1} - \hat{\boldsymbol{x}}_{k/k-1})(\boldsymbol{\chi}_{i,k/k-1} - \hat{\boldsymbol{x}}_{k/k-1})^T + \boldsymbol{Q}_k \tag{17}$$

where $\boldsymbol{\lambda}_k$ is the suboptimal fading factor. If the innovation vector is defined as:

$$\boldsymbol{e}_k = \boldsymbol{z}_k - \hat{\boldsymbol{z}}_{k/k-1} \tag{18}$$

The strong tracking filter must satisfy the two following conditions:

$$\begin{cases} E[(\boldsymbol{x}_k - \hat{\boldsymbol{x}}_k)(\boldsymbol{x}_k - \hat{\boldsymbol{x}}_k)^T] = \min \\ E[\boldsymbol{e}_k^T \boldsymbol{e}_{k+j}] = 0 \quad j = 1, 2, ... \end{cases} \tag{19}$$

where the first equation in (19) is the ultimate goal of the filter. The second equation in (19) is the orthogonality principle so that the helpful information can be extracted from the innovation sequence.

Suppose the estimation error and prediction error is defined as:

$$\tilde{\boldsymbol{x}}_k = \boldsymbol{x}_k - \hat{\boldsymbol{x}}_k \tag{20}$$

$$\tilde{\boldsymbol{x}}_{k/k-1} = \boldsymbol{x}_k - \hat{\boldsymbol{x}}_{k/k-1} \tag{21}$$

Submitting (4) and (7) into (21), $\tilde{\boldsymbol{x}}_{k/k-1}$ is changed to

$$\tilde{\boldsymbol{x}}_{k/k-1} = \boldsymbol{F}_k \tilde{\boldsymbol{x}}_{k-1} + \Delta(\tilde{\boldsymbol{x}}_{k-1}) + \boldsymbol{w}_k \tag{22}$$

where $\boldsymbol{F}_k = \partial f(\boldsymbol{x}) / \partial \boldsymbol{x}|_{x=\hat{x}_{k-1}}$ is the Jacobian matrix of the dynamical model $f(\cdot)$. $\Delta(\tilde{\boldsymbol{x}}_{k-1})$ denotes the high order term of Taylor expansion and the mismatch or abnormal disturbance. Thus, there exists the unknown diagonal matrix $\boldsymbol{\beta}_k = \text{diag}(\beta_{1,k}, \beta_{2,k}, ..., \beta_{n,k})$ satisfies the following condition:

$$\tilde{\boldsymbol{x}}_{k/k-1} = \boldsymbol{\beta}_k \boldsymbol{F}_k \tilde{\boldsymbol{x}}_{k-1} + \boldsymbol{w}_k \tag{23}$$

Submitting (4), (9) and (23) into (18), the innovation sequence is changed into:

$$\begin{aligned} \boldsymbol{e}_k &= \boldsymbol{z}_k - \hat{\boldsymbol{z}}_{k/k-1} \\ &= \boldsymbol{H}_k (\boldsymbol{x}_k - \hat{\boldsymbol{x}}_{k/k-1}) + \boldsymbol{v}_k \\ &= \boldsymbol{H}_k (\boldsymbol{\beta}_k \boldsymbol{F}_k \tilde{\boldsymbol{x}}_{k-1} + \boldsymbol{w}_k) + \boldsymbol{v}_k \end{aligned} \tag{24}$$

Thus, the corresponding innovation sequence $\boldsymbol{e}_{k+j}$ is defined as:

$$\boldsymbol{e}_{k+j} = \boldsymbol{H}_{k+j} (\boldsymbol{\beta}_{k+j} \boldsymbol{F}_{k+j} \tilde{\boldsymbol{x}}_{k+j-1} + \boldsymbol{w}_{k+j}) + \boldsymbol{v}_{k+j} \tag{25}$$

Submitting (24) and (25) into (19), the orthogonal matrix can be rewritten as:

$$\begin{aligned} \boldsymbol{V}_j &= E[\boldsymbol{e}_{k+j} \boldsymbol{e}_k^T] \\ &= E[(\boldsymbol{H}_{k+j} (\boldsymbol{\beta}_{k+j} \boldsymbol{F}_{k+j} \tilde{\boldsymbol{x}}_{k+j-1} + \boldsymbol{w}_{k+j}) + \boldsymbol{v}_{k+j})(\boldsymbol{H}_k (\boldsymbol{\beta}_k \boldsymbol{F}_k \tilde{\boldsymbol{x}}_{k-1} + \boldsymbol{w}_k) + \boldsymbol{v}_k)^T] \\ &= \boldsymbol{H}_{k+j} \boldsymbol{\beta}_{k+j} \boldsymbol{F}_{k+j} [\prod_{i=k+1}^{k+j-1} (\boldsymbol{I} - \boldsymbol{K}_i \boldsymbol{H}_i) \boldsymbol{\beta}_{k+j} \boldsymbol{F}_{k+j}] (\boldsymbol{P}_{xz} - \boldsymbol{K}_k \boldsymbol{V}_0) \end{aligned} \tag{26}$$

From (19), $\boldsymbol{V}_j = 0$, it can be deduced from (26) that

$$\boldsymbol{P}_{xz} - \boldsymbol{K}_k \boldsymbol{V}_0 = 0 \tag{27}$$

Submitting (11), (12) and (13) into (27), that is:

$$\boldsymbol{H}_k \boldsymbol{P}_{k/k-1} \boldsymbol{H}_k^T = \boldsymbol{V}_0 - \boldsymbol{R}_k \tag{28}$$

Submitting the modified prediction covariance $\hat{\boldsymbol{P}}_{k/k-1}^*$ in (17) into (28), we have

$$\boldsymbol{H}_k \lambda_k \sum_{i=0}^{2n} \omega_i (\boldsymbol{\chi}_{i,k/k-1} - \hat{\boldsymbol{x}}_{k/k-1})(\boldsymbol{\chi}_{i,k/k-1} - \hat{\boldsymbol{x}}_{k/k-1})^T \boldsymbol{H}_k^T = \boldsymbol{V}_0 - \boldsymbol{R}_k - \boldsymbol{H}_k \boldsymbol{Q}_k \boldsymbol{H}_k^T \tag{29}$$

where $\boldsymbol{V}_0$ actual innovation covariance output by the UKF and can be computed as:

$$\boldsymbol{V}_0 = \begin{cases} \boldsymbol{e}_1 \boldsymbol{e}_1^T & k = 1 \\ \dfrac{\rho \boldsymbol{V}_{k-1} + \boldsymbol{e}_k \boldsymbol{e}_k^T}{1+\rho} & k > 1 \end{cases} \tag{30}$$

where ρ $(0 < \rho \leq 1)$ is the forgetting factor and usually set to 0.95.

Seeking the trace of both sides in (29), the sub-optimal fading factor is obtained:

$$\lambda_k = \frac{\mathrm{tr}(\boldsymbol{V}_0 - \boldsymbol{R}_k - \boldsymbol{H}_k \boldsymbol{Q}_k \boldsymbol{H}_k^T)}{\mathrm{tr}(\boldsymbol{H}_k \sum_{i=0}^{2n} \omega_i (\boldsymbol{\chi}_{i,k/k-1} - \hat{\boldsymbol{x}}_{k/k-1})(\boldsymbol{\chi}_{i,k/k-1} - \hat{\boldsymbol{x}}_{k/k-1})^T \boldsymbol{H}_k^T)} \tag{31}$$

In order to avoid the situation that λ_k is less than 1, the sub-optimal fading factor can be revised as:

$$\lambda_k^* = \max(1, \lambda_k) \tag{32}$$

The flow chart of MSTUKF is shown in Figure 4 with the following steps:

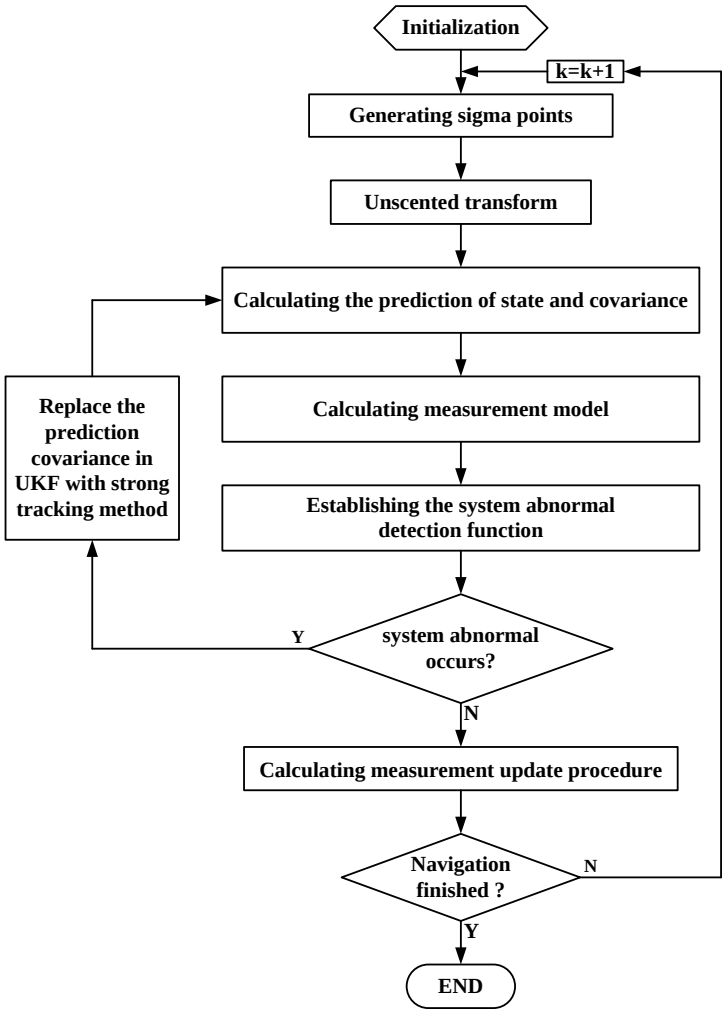

Figure 4. Flow Chart of MSTUKF

Step1: For the given state estimation $\hat{\boldsymbol{x}}_{k-1}$ and error covariance $\boldsymbol{P}_{k-1}$, the sigma point set is obtained with (5).

Step2: Each of the sigma points are calculated with the dynamical model so that the prediction mean $\hat{\boldsymbol{x}}_{k/k-1}$ and covariance $\boldsymbol{P}_{k/k-1}$ are obtained, which is described in (6)-(8).

Step3: The system state detection function is established based on the measurement residuals as illustrated in Section 3.1. If the uncertainty exists, return to Step 2 with the following two operations:

1) Replace the covariance $\boldsymbol{P}_{k/k-1}$ with $\boldsymbol{P}^{*}_{k/k-1}$ in (17).

2) Complete the prediction and update procedure in (9)-(14).

Otherwise, Complete the ordinary UKF procedure as (10)-(14).

Step 4: Repeat Step 1 to Step 3 for the next loop.

4. Simulation and Results Analysis

4.1. Simulation Conditions

In order to demonstrate the effectiveness of the proposed orbit determination method, two different scenarios are taken into consideration for simulating the dynamical model uncertainties. In each scenario, the MSTUKF is compared with UKF, AUKF and STUKF in the Earth-Mars transfer orbit. The simulation initial parameters are provided as follows:

1) Orbit element:

The orbit elements in the Earth-Mars transfer orbit are listed as follows [12]:

Semi-axis : 1.98×10^{8} km

Eccentricity : 0.236

Inclination : 23.455°

Right ascension of ascending node : 0.258°

Argument of perigee : 71.347°

True anomaly : 85.152°

2) Measurement parameter:

The pulsars PSR B1937+21, PSR B1821–24, and PSR B0531+21 are selected as the observed navigation pulsars and their parameters are listed in Table 1.

Table 1. Parameters of Adopted Pulsars

Pulsars	B0531+21	B1821-24	B1937+21
Right ascension [°]	**88.63**	**276.13**	**294.92**
Declination [°]	**22.01**	**-24.87**	**21.58**
Ranging accuracy [m]	**109**	**325**	**344**

3) Filtering parameter:

The measurement update in filtering algorithm is 500s. The beginning position and velocity errors are [6000m, 6000m, 6000m] and [2 m/s, 2 m/s, 2 m/s]. The initial error covariance $\boldsymbol{P}_0$, system noise covariance $\boldsymbol{Q}_k$ and measurement noise covariance $\boldsymbol{R}_k$ are:

$$\begin{cases} \boldsymbol{P}_0 = diag(6000^2, 6000^2, 6000^2, 2^2, 2^2, 2^2) \\ \boldsymbol{Q}_k = diag(2, 2, 2, 3^{-3}, 3^{-3}, 3^{-3}) \\ \boldsymbol{R}_k = diag(109^2, 325^2, 344^2) \end{cases} \tag{33}$$

Root mean square error is utilized to evaluate the navigation performance. Define the estimation error square root of position and velocity as

$$\begin{cases} \text{RMSE}_r = \sqrt{\sum_{j=1}^{M} \left\| \Delta \boldsymbol{r}_j \right\|^2} \\ \text{RMSE}_v = \sqrt{\sum_{j=1}^{M} \left\| \Delta \boldsymbol{v}_j \right\|^2} \end{cases} \tag{34}$$

where $\Delta \boldsymbol{r}$ and $\Delta \boldsymbol{v}$ are the estimation error of position and velocity. M is the length of the selected filtering interval.

4.2. Results Analysis

Scenario 1: Dynamical model mismatch. In this scenario, the dynamical model (2) is adopted in UKF, AUKF, STUKF and MSTUKF. However, the gravity of Jupiter and asteroid can still affect the accuracy of dynamical model. Thus, it clearly that the dynamical model is inaccurate because of the model mismatch. The performance of the four filtering algorithms are shown in Figure 5. With the increase of filtering, the estimation error of UKF is becoming larger. the UKF based method is sensitive dynamical model uncertainty caused by the model mismatch. While the corresponding estimation errors using AUKF, STUKF and MSTUKF are relatively convergent and stable. Obviously, the AUKF, STUKF and MSTUKF can effectively eliminate the influence of dynamical model mismatch.

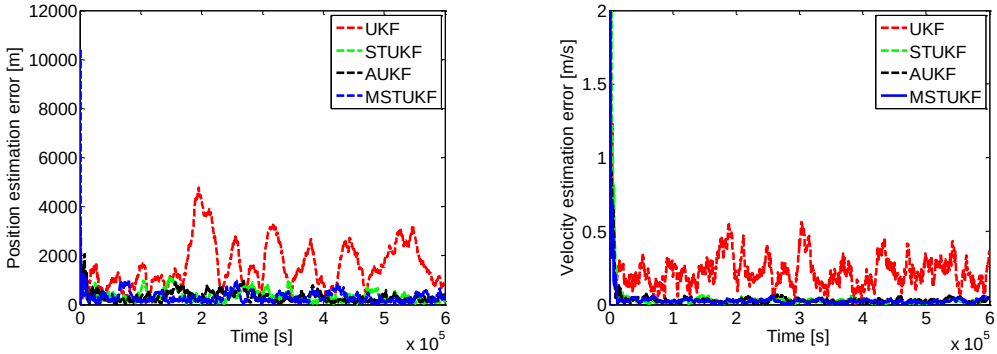

Figure 5. Position Estimation in Different Emphasis Error Levels

Scenario 2: Abnormal disturbance. In the second scenario, the abnormal disturbance is supposed to occur in the 2×10^5 second and lasts for 2500 seconds. The navigation results are shown in Figure 6. For the two filtering algorithms, both of them works well and is convergence from 0 to 2×10^5 the second. However, if the abnormal disturbance occurs, the performance of UKF is declined. The position and velocity estimation error increases to 4×10^3 meters and 0.5m/s, respectively. Then, the estimation error can return convergence after 8×10^4 seconds. For the AUKF and STUKF, the estimation error is smaller than UKF. However, the performances of the two filters are poor in the time intervals without abnormal disturbance. For the MSTUKF based method, the estimation error can convergence and keep stable state in the whole navigation procedure. That is to

say, the proposed MSTUKF based method can effectively reduce the influence of dynamical model uncertainty caused by abnormal disturbance.

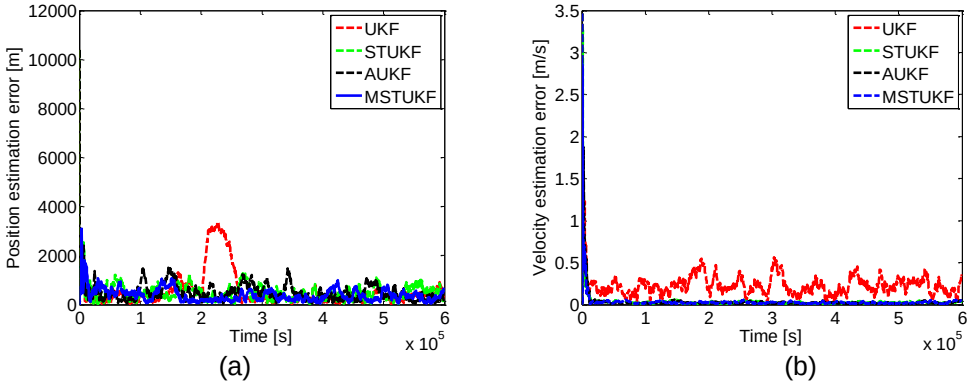

Figure 6. Position Estimation in Different Emphasis Error Levels

Table 2 shows the RMSE results of in the two cases using UKF and MSTUKF. In case 1, the RMSE is calculated in the time interval 2×10^5-6×10^5s. It is shown that compared with UKF, MSTUKF provides 82.3% and 91.4% improvement for position and velocity respectively. For the STUKF and AUKF, corresponding estimation error is improved by 80.4%, 91.5% and 77.9%, 90.6%. The reason is that the dynamical model mismatch exists in the whole filtering procedure, the performance of MSTUKF is similar to STUKF and AUKF.

Table 2. RMSE of the Two Filtering Methods

		Estimation error	
		$RMSE_r$ [m]	$RMSE_v$ [m/s]
Scenario 1	UKF	1865.7	0.2884
	AUKF	366.3	0.0244
	STUKF	412.1	0.0270
	MSTUKF	329.5	0.0248
Scenario 2	UKF	1962.6	0.1929
	AUKF	578.1	0.0317
	STUKF	529.5	0.0312
	MSTUKF	293.7	0.0265

In case 2, the RMSE is calculated for the 2×10^5s to 6×10^5 s. The estimation errors of position and velocity for MSTUKF are improved by 85.0% and 86.3%. While for the STUKF and AUKF, the corresponding estimation error are improved only by 73.0%, 83.9% and 70.5%, 83.6%. The improvement of the two filter's (STUKF and AUKF) performance is not as high as the MSTUKF's. This is because the STUKF and AUKF still utilize the suboptimal fading factor or adaptive factor in the time intervals where the process noise covariance is already accurate, leading to the degradation of the filter's performance. Thus, MSTUKF can achieve better performance than UKF and more suitable for the deep space exploration mission.

5. Conclusions

In this paper, a modified strong tracking UKF filtering algorithm is proposed to deal with the uncertainty exists in the dynamical model of XNAV. The influence of dynamical model to the conventional UKF is analyzed. The system state abnormal detection function

is established so that the influence to navigation system can be detected in case of the abnormal disturbance occurs. On the other hand, the prediction covariance is modified with the sub-optimal fading factor so that the filter gain can be revised. Compared with the UKF, AUKF and STUKF, the proposed method can effectively eliminate the impact of abnormal disturbance to dynamical model of XNAV and improve the navigation performance. The proposed method can be applied to transfer orbit with the unknow abnormal disturbance.

Acknowledgments

This work was supported by the innovation fund of China Aerospace Science and Technology Corporation-Harbin Institute of Technology Joint Innovation Center [CASC-HIT-1C04].

References

[1] A. A. Emadzadeh and J. L. Speyer, "X-ray pulsar-based relative naviation using epoch folding", IEEE Transactions on Aerospace Electronic Systems, vol. 47, no. 4, **(2011)**, pp. 2317-2328.
[2] A. Hewish, S. J. Bell, J. Pilkington, P. Scott and R. Collins, "Observation of a rapidly pulsating radio source", Nature., vol. 217, no. 5130, **(1968)**, pp. 709-713.
[3] L. Liu, W. Zheng and G. Tang, "Observability analysis of satellite constellations autonomous navigation based on X-ray pulsar measurement", Chinese Automation Congress, Changsha, China, **(2013)** November 7-8.
[4] Y. Wang, W. Zheng, S. Sun and L. Li, "X-ray pulsar based navigation using time-difference measurement", Aerospace science and technology., vol. 13, **(2014)**, pp. 27-35.
[5] L. Qiao, J. Liu, G. Zheng and Z. Xiong, "Augmentation of XNAV system to an ultraviolet sensor-based satellite navigation system", IEEE Journal of Selected Topics in Signal Processing, vol. 5, no. 3, **(2009)**, pp. 777-785.
[6] K. Xiong, C. Wei and L. Liu, "Robust Kalman filtering for discrete-time nonlinear systems with parameter uncertainties", Aerospace science and technology, vol. 18, (**2012**), pp. 15-24.
[7] J. Liu, J. Ma, J. Tian, Z. Kang and P. White, "Pulsar navigation for interplanetary missions using CV model and ASUKF", Aerospace science and technology, vol. 22, **(2012)**, pp. 19-23.
[8] J. Liu, J. Ma, J. Tian, Z. Kang and P. White, "X-ray pulsar navigation method for spacecraft with pulsar direction error", Advances in Space Research, vol. 46, **(2010)**, pp. 1409-1417.
[9] Y. Wang, W Zheng and S. Sun, "X-ray pulsar-based navigation system with the errors in the planetary ephemerides for Earth-orbiting satellite", Advances in Space Research, vol. 51, no. 12, **(2013)**, pp. 2394-2404.
[10] E. Wei, S. Jin, Q. Zhang, J. Liu, X. Li and W. Yan, "Autonomous navigation of Mars probe using X-ray pulsars: modeling and results", Advances in Space Research, vol. 51, **(2013)**, pp. 849-857.
[11] D. Feng, H. Guo, X. Wang and X. Yuan, "Autonomous orbit determination and its error analysis for deep space using X-ray pulsar", Aerospace Science and Technology, vol. 32, **(2014)**, pp. 35-41.
[12] J. Liu, J. Fang, Z. Yang, Z. Kang and J. Wu, "X-ray pulsar/Doppler difference integrated navigation for deep space exploration with unstable solar spectrum", Aerospace Science and Technology, vol. 41, **(2015)**, pp. 144-150.

